Title: Translational control of *MPS1* links protein synthesis with the initiation of cell division and spindle pole body duplication in yeast

Authors: Heidi M. Blank[1], Annabel Alonso[2], Mark Winey[2,3], Michael Polymenis[1,3]

Affiliations: [1]Department of Biochemistry and Biophysics, Texas A&M University, College Station, TX, USA

[2]Department of Molecular and Cellular Biology, University of California, Davis, Davis, CA 95616

[3]**Contact:** mwiney@ucdavis.edu; polymenis@tamu.edu

Key words: SPB, MTOC, cell size, SIM, *Saccharomyces cerevisiae*

ABSTRACT

Protein synthesis underpins cell growth and controls when cells commit to a new round of cell division at a point in late G1 of the cell cycle called Start. Passage through Start also coincides with the duplication of the microtubule-organizing centers, the yeast spindle pole bodies, which will form the two poles of the mitotic spindle that segregates the chromosomes in mitosis. The conserved Mps1p kinase governs the duplication of the spindle pole body in *Saccharomyces cerevisiae*. Here, we show that the *MPS1* transcript has a short upstream open reading frame that represses the synthesis of Mps1p. Mutating the *MPS1* uORF makes the cells smaller, accelerates the appearance of Mps1p in late G1, and promotes completion of Start. The accelerated Start of *MPS1* uORF mutants depends on the G1 cyclin Cln3p. Monitoring the spindle pole body in the cell cycle using structured illumination microscopy revealed that mutating the *MPS1* uORF enabled cells to duplicate their spindle pole body earlier, at a smaller cell size. For the first time, these results identify growth inputs in mechanisms that control duplication of the microtubule-organizing center and implicate these processes in general mechanisms that couple growth with division.

INTRODUCTION

Basic cellular parameters, such as cell size and macromolecular composition, do not change much throughout successive cell divisions, and cell growth and division appear balanced with each other. The rate at which cells can divide usually depends not on how fast they can replicate their genome but on how fast they can synthesize everything else that goes into a newborn cell (Johnston *et al.*, 1977). Newborn budding yeast daughter cells actively control when they begin replicating their genome in response to their growth status. They stay in the G1 phase of the cell cycle until they reach a characteristic threshold of cell growth, known as critical size (Hartwell and Unger, 1977; Di Talia *et al.*, 2007). The protein synthesis rate is thought to underpin overall cell growth and determine when cells will reach their critical size and commit to a new round of DNA replication at a point in late G1, called Start (Polymenis and Aramayo, 2015). Translational control of *CLN3*, encoding a G1 cyclin, alters the timing of Start in different nutrients (Polymenis and Schmidt, 1997; Blank *et al.*, 2018), and synthesis of Cln3p in G1 may respond to a critical rate of protein synthesis (Litsios *et al.*, 2019). However, other molecular targets that could impose the protein synthesis requirements for cell division initiation have remained elusive.

The spindle pole body (SPB) of yeast is a large protein organelle serving the same role as the centrosome in animals. The two SPBs in mitosis form the two poles from which all the microtubules of the mitotic spindle originate (Jaspersen and Winey, 2004). The SPB is embedded in the nuclear envelope, and it is a stack of three major protein layers or plaques. Besides the chromosomes, the SPB is the only large macromolecular complex present in a single copy early in the G1 phase of the cell cycle. By the time cells pass through Start, a protein extension of the middle plaque, called the half-bridge, nucleates the new SPB formation, which then matures and separates from the old SPB. From classical experiments involving loss-of-function mutants, it is thought that passage through Start is required for SPB duplication and not the other way around (Hartwell *et al.*, 1974; Pringle, 1981).

Mps1p is a conserved protein serine, threonine, and tyrosine kinase required for SPB duplication (Winey *et al.*, 1991; Lauzé *et al.*, 1995; Liu and Winey, 2012). Mps1p also regulates various other mitotic events, most prominently bipolar chromosome attachment and the spindle checkpoint (Liu and Winey, 2012). Post-translational mechanisms control Mps1p's levels (through proteolysis), activity (through phosphorylation by several kinases, including by Mps1p itself), and localization (at least in part through phosphorylation and localized degradation) in the cell (Liu and Winey, 2012). Mps1p abundance is very low, at ~500 molecules/cell in asynchronous cells (Ho *et al.*, 2018). Mps1p levels peak in metaphase, consistent with Mps1p's numerous mitotic roles, but then the anaphase-promoting complex destroys Mps1p for a timely mitotic exit (Palframan *et al.*, 2006). Over-expression of Mps1p arrests cells in mitosis (Hardwick *et al.*, 1996). How Mps1p levels are controlled in G1 is unknown.

We had previously identified *MPS1* as one of a few mRNAs whose translational efficiency changes in the cell cycle (Blank *et al.*, 2017). Here, we identify a short upstream open reading frame (uORF) in *MPS1*. Mutating the *MPS1* uORF caused an earlier appearance of Mps1p in G1 and accelerated SPB duplication. It also reduced the critical size for Start completion, in a Cln3p-dependent manner. These results reveal direct growth and protein synthesis inputs in the Mps1p-controlled SPB cycle. They also show that SPB-related processes can actively determine when cells commit to a new round of cell division at Start.

RESULTS AND DISCUSSION

Mutating a conserved uORF in *MPS1* reduces cell size

To test the role of translational control in Mps1p synthesis, we looked at possible *cis-elements* in the *MPS1* mRNA that could mediate that control. The 5'-leader of *MPS1* is 133 nt-long (Poch *et al.*, 1994), and has a uORF (Figure S1, top). The uORF initiates 17 nt upstream but overlaps and terminates past the main *MPS1* start codon (Figure S1). Hence, the uORF could repress the translation of *MPS1* because ribosomes that synthesize the uORF-encoded peptide will bypass the *MPS1* start codon. A uORF at the same position, albeit of varying length and sequence, is present in other *Saccharomyces* genomes (Figure S1). Based on aggregate ribosome profiling experiments from the literature, it appears that the uORF sequences are bound by ribosomes (Michel *et al.*, 2014), suggesting that the uORF is translated.

To test the role of the *MPS1* uORF, we mutated its start codon in two different ways (Figure 1A). The 5'-leader may also be structured (Figure S2). The uORF mutations we introduced may (*uORFm1-MPS1*) or not (*uORFm2-MPS1*) alter the predicted 5'-leader structure (Figure S2). The two different mutants provide independent means to test the role of the *MPS1* uORF. The mutations were introduced in their native surrounding context in the chromosome, with the endogenous *MPS1* promoter driving the *MPS1* mRNA expression (see Material and Methods). For protein surveillance experiments, we also introduced a C-terminal TAP tag to visualize Mps1p-TAP on immunoblots (see Material and Methods).

While both *MPS1* uORF mutants proliferated at the same rate as their *uORF*$^{+}$ counterpart, we noticed that they had a small overall cell size, regardless of strain background (BY4741 in Figure 1B; W303 - Figure 1C). The cells were born at the right size (Figure 1C, left panel), but the mean size of asynchronously proliferating cells was about 10-15% smaller (Figure 1C, right panel; $p<0.005$ based on the non-parametric Kruskal-Wallis and the posthoc Nemenyi tests). The uORF mutations did not appear to change the steady-state levels of *MPS1* mRNA or Mps1-TAP protein in asynchronous cells (Figure S3). This is not surprising due to the

known mechanisms that regulate Mps1p abundance in the cell cycle, as we will describe in the next section. However, the smaller mean cell size of asynchronous cultures of the *MPS1* uORF mutants was interesting and suggestive of cell cycle-dependent phenotypes, which we examined next.

Mutating the *MPS1* uORF accelerates the appearance of Mps1p in the cell cycle and promotes Start

Smaller cell size is often associated with accelerated completion of Start, as was shown initially for stabilized, gain-of-function mutants of the G1 cyclin Cln3p (Sudbery *et al.*, 1980; Cross, 1988). To measure the timing of Start in the *MPS1* uORF mutants, we obtained highly synchronous cultures by centrifugal elutriation, which maintains as much as possible the coordination of cell growth with division (Creanor and Mitchison, 1979; Aramayo and Polymenis, 2017). The abundance of Mps1p in elutriated daughter cells has not been measured in past studies. We found that Mps1p-TAP is absent in G1 and begins accumulating at the G1/S transition when cells begin budding (Figure 2A, top panel). This is expected because Mps1p is a substrate of the anaphase-promoting complex (APC) (Palframan *et al.*, 2006), and the APC is active in G1. Mps1p-TAP levels peak late in the cell cycle, in mitosis, when the percentage of budded cells is the highest (>90%), and then Mps1 levels drop again as cells exit mitosis (Figure 2A, B). In both independently constructed *MPS1* uORF mutants, Mps1p-TAP abundance was also periodic, absent in G1 and peaking late in the cell cycle (Figure 2A, B). However, Mps1p-TAP began appearing in smaller cells (~5 fL smaller) in the *MPS1* uORF mutants than wild-type cells (Figure 2A, B). Hence, although mutating the *MPS1* uORF does not change the steady-state levels of Mps1p in asynchronous cells (Figure S3), it changes the kinetics of the Mps1p appearance in the cell cycle (Figure 2).

Budding yeast daughter cells commit to a new round of DNA replication when they reach a critical size threshold at Start. Since budding coincides with the initiation of DNA replication in

yeast (Hartwell *et al.*, 1974), from such synchronous elutriated cultures, the critical size is commonly defined as the size at which half the cells are budded. Remarkably, the critical size of *MPS1* uORF mutants was ~40 fL, while that of wild type cells was >45 fL (Figure 2C; e.g., the critical size is reduced by 9% (Wilcoxon rank-sum test; p-value = 0.0005828) in the *uORFm1-MPS1* mutant). Hence, Start was accelerated in the *MPS1* uORF mutants.

The smaller mean and critical size of *MPS1* uORF mutants depends on the G1 cyclin Cln3p

Two critical regulators of Start in yeast are the G1 cyclin Cln3p (promotes Start) and Whi5p (inhibits Start). Whi5p is a transcriptional repressor, analogous with the retinoblastoma (Rb) gene product of animal cells (Costanzo *et al.*, 2004; de Bruin *et al.*, 2004). Removing Cln3p makes the cells bigger (Cross, 1988; Nash *et al.*, 1988) while removing Whip5 makes them smaller (Costanzo *et al.*, 2004; de Bruin *et al.*, 2004). Cells lacking Whi5p are among the smallest-sized mutants in yeast (Jorgensen *et al.*, 2002). Yet introducing the *uORFm1-MPS1* allele in *whi5Δ* cells made them even smaller (Figure 3A). On the other hand, mutating the *MPS1* uORF did not reduce the size of *cln3Δ* cells (Figure 3A). We tested further the dependence of Mps1p on Cln3p, by measuring the timing of Start in synchronous, elutriated cultures. The critical size threshold for Start is greatly delayed in cells lacking Cln3p (at 80 fL, compared to 46 fL for wild type cells; Figure 3B), and it was not accelerated at all in double, *uORFm1-MPS1, cln3Δ* mutants (Figure 3B). These results suggest that when the *MPS1* uORF is mutated, it may be Cln3p, but not Whi5p, that is needed for Mps1p to reduce cell size.

Reducing the translational efficiency of *MPS1* accelerates SPB duplication in synchronous, elutriated cells.

Since the timing of Start was altered in *MPS1 uORF* mutants (Figure 2), and Mps1p plays multiple roles in SBP duplication, we examined the effect of the *uORFm1-MPS1* mutation on the

timing of morphological landmarks of the SBP cycle. Note that cells continue to grow during a cell cycle block, and when they are released from their arrest, they typically progress quickly through the G1 phase of the cycle. In contrast, early G1 cells obtained by centrifugal elutriation are not arrested and must meet their growth requirements for Start. Hence, synchronous cultures obtained by centrifugal elutriation enable the monitoring of early G1 events. To our knowledge, the SPB cycle has not been followed in elutriated synchronous cultures starting in early G1.

To visualize SPB duplication's early steps, we used a strain harboring two fluorescently tagged SPB components, *Spc42p-GFP* and *Spc110p-tomato*. Spc42p is a central plaque component of the SPB (Bullitt *et al.*, 1997), which is phosphorylated by Mps1p (Castillo *et al.*, 2002). Spc110p is an inner plaque SPB component, which attaches γ-tubulin to the SPB, and Mps1p also phosphorylates Spc110p (Friedman *et al.*, 2001). Early G1 cells of this strain were obtained by elutriation and monitored at regular intervals for cell size, budding, and samples were fixed for SPB analysis by structured illumination microscopy (SIM) (Figure 4). The single SPB has a half-bridge attached, which doubles in length once SPB duplication commences (Li *et al.*, 2006). Once the half-bridge elongates, proteins assemble at the distal end of the bridge to form a precursor to a new SPB, called a satellite (Winey and Bloom, 2012). Spc42p is one of several proteins deposited at the satellite location. This event is viewed as a cone-like structure flaring off the original SPB, denoted as 'satellite-early' in Figure 4. When most of the cells are unbudded, the prominent SBP feature seen is one SBP alone or one SPB with a small cone process indicating early satellite body formation (Figure 4). Shortly before the size at which budding occurs in *uORF*$^{+}$*-MPS1* cells, fully formed satellite processes are detected, denoted as 'satellite-late' in Figure 4. The appearance of duplicated, side-by-side SBPs is detected once the cells bud and pass through Start (Figure 4). The final step, separation of the SPBs, occurs during anaphase of mitosis, consistent with our data showing this separation occurring near the end of the cell cycle (Figure 4). These data describe the morphology of early events of the SPB

cycle in highly synchronous, elutriated newborn daughter cells, documenting the formation of early satellite structures soon after birth.

We introduced the *uORFm1-MPS1* allele in the *SPC42-GFP*, *SPC110-tomato* strain, and measured the timing of the above event of the SPB cycle. Using again cell size as a proxy for cell cycle position, it appears that the early steps of the SPB occur at the same time in the *uORFm1-MPS1* mutant and *uORF*$^{+}$*-MPS1* cells. For example, the appearance of cells with satellite-late morphology peaks at 40 fL in both strains (Figure 4A). However, *uORFm1-MPS1* cells peak with SPB duplicated morphology soon after, at a size of ~42 fL. In contrast, the *uORF*$^{+}$*-MPS1* cells do so at a larger cell size (47-48 fL, compare the second row panels in Figure 4A). The subsequent step of cell separation is also accelerated in *uORFm1-MPS1* cells compared to *uORF*$^{+}$*-MPS1* ones (Figure 4A, compare the two top panels). These results show that cells that do not have the *MPS1* uORF duplicate their SPB earlier, at a smaller size.

The role of centrosomes in cell division is as old as the chromosome theory of heredity, with centrosome amplification a common feature of cancers (Boveri, 2008). Normally, centrosome and SPB duplication are entrained with the master cell cycle switch governed by the activity of cyclin-dependent kinase (Cdk) (Jaspersen and Winey, 2004; Nigg and Raff, 2009). In some cases, however, they can duplicate independently of cell-cycle progression (Nigg and Raff, 2009). In animals, autonomous oscillations of the polo-like kinase Plk4 can drive centrosome duplication independently of Cdk (Aydogan *et al.*, 2020). Intriguingly, centriole growth in the cell cycles of fly embryos appears to follow a homeostatic ‘sizer-like’ model, actively monitoring and adjusting their growth until they reach the proper size (Aydogan *et al.*, 2018). An analogous mechanism has not been shown for the budding yeast SPB. However, the same principle operates during the G1 phase of daughter cells to control Cdk activity before cells commit at Start to initiate budding and DNA replication (Hartwell and Unger, 1977; Di Talia *et al.*, 2007). Our results argue that through translational control of *MPS1*, growth and protein synthesis also directly trigger SPB duplication, expanding the range of growth inputs the cell

uses to control the timing of Start. Hence, monitoring the growth and duplication of the SPB/centrosome may contribute to the overall coupling of cell growth with division in proliferating cells.

MATERIAL AND METHODS

Key resources table

Reagent type (species) or resource	Designation	Source or reference	Identifiers	Additional information
antibody	Peroxidase Anti-Peroxidase (PAP) Soluble Complex	Sigma-Aldrich	P1291	(1:1000)
antibody	Anti-Pgk1p antibody, rabbit polyclonal	Novex by Life Technologies	459250	(1:1000)
antibody	Alexa Fluor® 488 AffiniPure Goat Anti-Mouse IgG (H+L)	Jackson Immunoresearch Laboratories	115-545-003	(1:1500)
chemical compound, drug	Dextrose	Sigma-Aldrich	D9434	
chemical compound, drug	Zymolyase 20T	MP biomedicals	SKU 08320921	
chemical compound, drug	Tris (hydroxymethyl) aminomethane	Sigma-Aldrich	252859	
chemical compound, drug	Tris base	Roche	TRIS-RO	
chemical compound, drug	Sodium chloride	Sigma-Aldrich	S7653	
chemical compound, drug	Magnesium chloride hexahydrate	USP	1374248	
chemical compound, drug	DTT	Sigma-Aldrich	D0632	
chemical compound,	Triton™ X-100	Sigma-Aldrich	T8787	

drug				
chemical compound, drug	Phosphate buffered saline (PBS)	Sigma-Aldrich	P4417	
chemical compound, fixation	Paraformaldehyde, 16%	Ted Pella, Inc.	18505	SIM microscopy
Commercial assay, kit	One step RT-ddPCR Advanced kit for probes	Bio-Rad	1864021	RNA surveillance
other	BioTrace™ NT nitrocellulose	Pall Corporation	66485	Immunoblotting
other	Immobilon®-FL membrane	MilliporeSigma	IPFL07810	Immunoblotting
other	Mini-PROTEAN® TGX Stain-Free™ Gels, 4-15%	Bio-Rad	4568086	Immunoblotting
other	Yeast extract	Sigma-Aldrich	Y1625	
other	Peptone	Sigma-Aldrich	P5905	
other	Glass beads	Scientific Industries	SI-BG05	
other	ProLong™ Gold Antifade Mountant	ThermoFisher Scientific	P36934	SIM microscopy
Sequence based reagent	IV403709-F1			TCTGGAGAATTCTTTTCAAAATATAACATTTCAAAAATAAACGACAAAAACACTGAATACCGGATCCCCGGGTTAATTAA
Sequence based reagent	IV403709-R1			AAATTGTGGCATCACAGTAATGCTCAAACAAAAACTTTAATGTTCTTTACTCTTTTAGGGGAATTCGAGCTCGTTTAAAC
Sequence based reagent	IV403783-FWD			CAACAAATGGTGATTCTGGAG
Sequence based reagent	IV403164-REV			TGGGAAAGTAAAGCTGATCCG
Sequence based reagent	pBS1539	(Puig et al)		C- terminal TAP fusion plasmid
Sequence based reagent	AT-17TA-MPS1-REV			CTCGATTTTAAATCCACATAATCATGGAATGAGTTTGTTGACATGTTTGTTTTGAGATCTACCAGTTCTTGCAGAAAC

Sequence based reagent	uORFm2-MPS1-REV			GAGTTTGTTGACATGTTTGTTTTGAGATTTTTCAGTTCTTGCAGAAACAATTTATTATTTTGGTTGTAAAGCTACTTCTATAAACAACTGCAATATTCCTATTC
Sequence based reagent	IV403783-FWD			CAACAAATGGTGATTCTGGAG
Sequence based reagent	IV403638-FWD			CATGTTTATATATTCTGACCA
Sequence based reagent	IV403164-REV			TGGGAAAGTAAAGCTGATCCG
Sequence based reagent	IV403783-FWD			CAACAAATGGTGATTCTGGAG
Sequence based reagent	MPS1-CTAP-FWD			GATGATCTCAATGATGTGGTAGACACTGTTTTAAGGAAATTTGCAGATTACAAAATTTCCATGGAAAAGAGAAG
Sequence based reagent	MPS1-CTAP-REV			AAACTCTAAATGTATTTATGTTCATAACTGGCACATGCTTTTCTTCCTTATGCGGCTCTTTACGACTCACTATAGGG
Sequence based reagent	MPS1-FAM-probe	Sc04106277_s1, Cat#4448892	Thermo Fisher Scientific	RNA surveillance
Sequence based reagent	UBC6-VIC-probe	Sc04118595_s1, Cat# 4351372	Thermo Fisher Scientific	RNA surveillance
software, algorithm	AccuComp Z2	Beckman Coulter	383550	Software to monitor number and size of cells with Z2 cell counter
Software, algorithm	QuantaSoft™ Software	Bio-Rad		Software to determine the concentration of transcript abundance by ddPCR
software, algorithm	ImageJ	https://imagej.net/	RRID:SCR_003070	Image processing software
software, algorithm	Adobe Photoshop	https://www.adobe.com/products/photoshop.html	RRID:SCR_014199	Image processing software
software, algorithm	RStudio	http://www.rstudio.com/	RRID:SCR_000432	Software for the R statistical computing environment
software, algorithm	SGD	http://www.yeastgenome.org/	RRID:SCR_004694	Saccharomyces Genome Database

software, algorithm	R	https://www.r-project.org	v3.6.3 RRID:SCR_001905	Statistical Computing Environment
strain, strain background (S. cerevisiae)	BY4743	(Giaever et al., 2002)	RRID:SCR_003093	MATa/α his3Δ1/his3Δ1 leu2Δ0/leu2Δ0 LYS2/lys2Δ0 met15Δ0/MET15 ura3Δ0/ura3Δ0
strain, strain background (S. cerevisiae)	BY4741	(Giaever et al., 2002)	RRID:SCR_003093	MATa his3Δ1 leu2Δ0 met15Δ0 ura3Δ0
strain, strain background (S. cerevisiae)	BY4741	Horizon Discovery TAP tagged ORF collection	Catalog ID:YSC1178-202230172	MATa his3Δ1 leu2Δ0 met15Δ0 ura3Δ0 MPS1-TAP::HIS3MX6
strain, strain background (S. cerevisiae)	W303a			MATa leu2-3,112 trp1-1 can1-100 ura3-1 ade2-1 his3-11,15
strain, strain background (S. cerevisiae)	W303	This study (HB68)	Horizon strain backcrossed 3x to W303	MATa leu2-3,112 TRP+ can1-100 ura3-1 ADE2+ his3-11,15, MPS1-TAP::HIS3MX6
strain, strain background (S. cerevisiae)	W303	This study (HB67)	Horizon strain backcrossed 3x to W303	MATα leu2-3,112 TRP+ can1-100 ura3-1 ADE2+ his3-11,15, MPS1-TAP::HIS3MX6
strain, strain background (S. cerevisiae)	BY4741	This study (HB48)		MATa his3Δ1 leu2Δ0 met15Δ0 ura3Δ0 KanMX-uORFm1-MPS1-TAP::URA3
strain, strain background (S. cerevisiae)	W303	This study (HB53)	HB48 backcrossed 3x to W303	MATα leu2-3,112 trp1-1 can1-100 ura3-1 ADE2+ his3-11,15 KanMX-uORFm1-MPS1-TAP::URA3
strain, strain background (S. cerevisiae)	W303	This study (uORFm1-MPS; HB49)	HB48 backcrossed 3x to W303	MATa leu2-3,112 trp1-1 can1-100 ura3-1 ADE2+ his3-11,15 KanMX-uORFm1-MPS1-TAP::URA3
strain, strain background (S. cerevisiae)	W303	This study (uORFm2-MPS1; HB219)		MATa leu2-3,112 trp1-1 can1-100 ura3-1 ade2-1 his3-11,15 KanMX-uORFm2-MPS1-TAP::URA3
strain, strain	W303	This study (HB99)	HB67 x	MATa leu2-3,112 TRP+

background (S. cerevisiae)			MWY5264	can1-100 ura3-1 ADE2+ his3-11,15 MPS1-TAP::HIS SPC42-GFP::KanMX SPC110-tomato::HIS3
strain, strain background (S. cerevisiae)	W303	This study (HB263)	HB53 x MWY5264	MATa leu2-3,112 trp1-1 can1-100 ura3-1 ADE2+ his3-11,15 KanMX-uORFm1-MPS1-TAP::URA3 SPC42-GFP::KanMX SPC110-tomato::HIS3
strain, strain background (S. cerevisiae)	W303	Winey lab collection	MWY5264	MATα leu2-3,112 trp1-1 can1-100 ura3-1 ADE2+ his3-11,15 SPC42-GFP::KanMX SPC110-tomato::HIS3
strain, strain background (S. cerevisiae)	BY4741	This study (HB173, HB176)	HB48 x cln3Δ::kanMX	MATa his3Δ1 leu2Δ0 met15Δ0 ura3Δ0 cln3Δ::kanMX kanMX-uORFm1-MPS1-TAP::URA3
strain, strain background (S. cerevisiae)	BY4741	This study (HB177)	MPS1-TAP-HISMX6 x cln3Δ::kanMX	MATa his3Δ1 leu2Δ0 met15Δ0 ura3Δ0 cln3Δ::kanMX MPS1-TAP::HIS3MX6
strain, strain background (S. cerevisiae)	BY4741	This study (HB169, HB170)	MPS1-TAP-HIS3MX6 x whi5Δ::kanMX	MATa his3Δ1 leu2Δ0 met15Δ0 ura3Δ0 whi5Δ::KanMX MPS1-TAP::HIS3MX6
strain, strain background (S. cerevisiae)	BY4741	This study (HB174, HB175)	HB48 x whi5Δ::kanMX6	MATa his3Δ1 leu2Δ0 met15Δ0 ura3Δ0 whi5Δ::kanMX6 KanMX6-uORFm1-MPS1-TAP::URA3
strain, strain background (S. cerevisiae)	BY4743	This study (MSP238)		KanMX-MPS1/MPS1, BY4743 otherwise
strain, strain background (S. cerevisiae)	BY4743	This study (MSP239)		KanMX-uORFm1-MPS1/MPS1, BY4743 otherwise
strain, strain background (S. cerevisiae)	BY4741	This study (MSP240-3C)		KanMX-MPS1, BY4741 otherwise
strain, strain background (S. cerevisiae)	BY4741	This study (MSP241-1C)		KanMX-uORFm1-MPS1, BY4741 otherwise

Where known, the Research Resource Identifiers (RRIDs) are shown.

Strains and media

All the strains used in this study are shown in the Key Resources Table, above. Unless noted otherwise, the cells were cultivated in the standard, rich, undefined medium YPD (1% $^{w}/_{v}$ yeast extract, 2% $^{w}/_{v}$ peptone, 2% $^{w}/_{v}$ dextrose), at 30°C (Kaiser *et al.*, 1994).

To modify the *MPS1*-5' leader, we first inserted a *KanMX6* cassette upstream, at position ChrIV:403709 with the PCR-mediated methodology of (Longtine *et al.*, 1998), using primers IV403709-F1 and IV403709-R1 (see Key Resources Table). The PCR product was introduced into strain BY4743, to generate the heterozygous strain MSP238, which was sporulated and dissected to generate the haploid MATα (MSP240-3A) and MATa (MSP240-3C) segregants. The *KanMX6* insertion was verified by PCR, using primers IV403783-FWD and IV403164-REV.

To introduce the uORFm1 mutation, we used primers IV403783-FWD and AT-17TA-MPS1-REV in a PCR reaction with genomic DNA from MSP240-3A. The PCR product was then used to transform strain BY4743, to generate strain MSP239. Introduction of the uORFm1 was initially verified by restriction digestion, since the uORFm1 introduces a BglII restriction site. Strain MSP239 was then sporulated and dissected to generate the haploid uORFm1 haploid MATa (MSP240-1C) segregant. The uORFm1 mutation was verified by sequencing with primers IV403638-FWD and IV403164-REV.

To insert a C-terminal TAP tag at the *MPS1* locus, we amplified the TAP-tagged sequences from plasmid pBS1539 (Puig *et al.*, 2001) with primers MPS1-CTAP-FWD and MPS1-CTAP-REV, and used the PCR product to transform the above generated *uORF*$^{+}$*-MPS1* and *uORFm1-MPS1* haploid strains. These BY4741-based strains were then crossed with W303α three times to generate the equivalent W303-based strains.

For construction of the uORFm2-MPS1-TAP strain, primers uORFm2-MPS1-REV and IV403783-FWD were used in a PCR reaction, using as template genomic DNA of a uORFm1-MPS1-TAP strain. The generated PCR product contained the KanMX cassette and introduced the point mutations at the uORF of *MPS1* shown in Figure 1. This PCR product was transformed into W303a cells, and potential candidates were sequenced with primers IV403638-FWD and IV403164-REV to confirm the presence of the uORF mutations. Verified uORFm2 strains were then transformed again with the PCR product of primer pair MPS1-CTAP-FWD and MPS1-CTAP-REV with DNA extracted from the uORFm1 strain to insert the TAP protein tag. All transformed strains were backcrossed once.

Construction of the fluorescently tagged strains for SIM microscopy was accomplished by crossing strain MWY5624 with the strains carrying the appropriate TAP-tagged *uORF*$^{+}$*-MPS1* or *uORFm1-MPS1* allele. Since these crosses involved multiple genes tagged with the same marker, the obtained tetrads were analyzed carefully to pick non parental ditypes of the double genetic markers. Strains were further confirmed by immunoblotting for the presence of Mps1p-TAP, and the presence of both fluorescent markers was confirmed microscopically.

Sample-size and replicates

For sample-size estimation, no explicit power analysis was used. All the replicates in every experiment shown were biological ones, from independent cultures. A minimum of three biological replicates was analyzed in each case, as indicated in each corresponding figure's legends. Where three replicates were the minimum number of samples analyzed, the robust bootstrap ANOVA was used to compare different populations via the t1waybt function, and the posthoc tests via the mcppb20 function, of the WRS2 R language package (Wilcox, 2011; Mair and Wilcox, 2016). For measurements where at least four independent replicates were analyzed, we used nonparametric statistical methods, as indicated in each case. No data or outliers were excluded from any analysis.

Centrifugal elutriation and cell size measurements

For each elutriation experiment in YPD (1% $^{w}/_{v}$ yeast extract, 2% $^{w}/_{v}$ peptone, 2% $^{w}/_{v}$ dextrose, plus 0.02 g/L of adenine for strains of W303 background), a 350 mL culture was allowed to reach a density of 1-5E+07 cells/mL. Cells were loaded at a 35 mL/min pump speed onto a large elutriator chamber (40 mL), spinning at 3,200 rpm (Beckman J-6M/E centrifuge). The centrifuge chamber was set at 4°C during all centrifugation steps until approximately 10 min before cell harvesting, when the temperature was increased to avoid the refrigeration from turning on and disrupting the cell gradient in the chamber. For typical time-series experiments with synchronous elutriated cultures (e.g., see Figure 2A), we isolated the first, early G1 daughter fraction and monitored it at regular intervals afterward as it progressed in the cell cycle, as we have described elsewhere (Hoose *et al.*, 2012; Soma *et al.*, 2014).

Protein surveillance

Protein extracts for immunoblots were made with the sodium hydroxide extraction method described previously (Amberg *et al.*, 2006). The extracts from synchronous culture samples were run on 10% Tris-Glycine SDS–PAGE gels and transferred to a nitrocellulose membrane. For detection of proteins of interest on immunoblots, we used an anti-Pgk1p antibody to detect Pgk1p and the peroxidase-anti-peroxidase (PAP) soluble complex to detect TAP-tagged proteins. Chemiluminescence reagents were from Thermo Scientific and used at the dilutions recommended by the manufacturer for detection of the TAP-tagged Mps1p. A secondary antibody was used to detect Pgk1p (Jackson Immunoresearch Laboratories). Detection of the proteins was digitally acquired using an Amersham™ Imager 600 (GE Healthcare).

The extracts from batch cultures were prepared the same as above but instead ran on Mini-PROTEAN® TGX Stain-Free™ Gels and transferred to a low-fluorescence PVDF membrane. Protein detection was as above, but using the stain-free gel technology, we could

acquire a total protein image of the blot to be used as an additional loading control along with Pgk1p. The manufacturer's instructions were followed to activate the gel, except using an Amersham™ Imager (GE Healthcare) for 3 minutes to activate the gel after completion of electrophoresis. Following transfer to an Immobilon®-FL membrane, the total protein was detected using the UV channel of the Amersham™ Imager 600. Images were processed with the "Subtract Background" tool, and band intensities quantified using the "Measure" tool to obtain a mean intensity for each band, using the ImageJ software package. The area measured was kept constant for a particular sample series for each blot analyzed.

To calculate the Log2(expressed ratios) in cell cycle series (e.g., see Figure 2), for any one protein of interest (Mps1p-TAP or Pgk1p), each signal value was divided by the average signal across the entire cell cycle series for that protein. These ratios were then Log2-transformed and reported on the y-axis.

Transcript abundance using digital droplet PCR (ddPCR)

For RNA surveillance, RNA extracts were made as described previously (Blank *et al.*, 2020). Briefly, RNA was extracted using the hot acidic phenol method. Cell pellets were resuspended in 0.4 ml of TES buffer (10 mM Tris, pH 7.5; 10 mM EDTA, and 0.5% SDS) with 0.1 ml of glass beads. Then, 0.4 ml of acid phenol, pH 4.5, was added, and the samples were heated at 65°C for 0.5 h with occasional vortexing for 10 s each time. The samples were then centrifuged for 5 m at 13,000 g. The aqueous layer was transferred to a new tube containing 1 ml of cold 100% ethanol with 40 µl of 3 M sodium acetate and incubated overnight at 4°C. The next day, the samples were centrifuged at 13,000 g for 20 min at 4°C, washed with 80% ethanol, and centrifuged again for 5 min at 13,000 g. The pellets were resuspended in 25 µl water. The amount of total RNA in each sample was measured with a ThermoFisher NanoDrop™ spectrophotometer. For the quantification of transcript abundance, 1 ng of total RNA was used for each sample.

The ddPCR reaction mixture was prepared by following the manufacturer's protocol (One-Step RT-ddPCR Advanced Kit for Probes), using the TaqMan® hydrolysis probes labeled with FAM-MBP for MPS1 and VIC-MBP for UBC6 reporter fluorophores. The mixture was kept on ice throughout the whole experiment. Once the reaction mixture was prepared, the samples were placed into a droplet generator (QX200™ AutoDG™ Droplet Digital™ PCR System), which uses specially developed reagents and microfluidics to partition each sample into 20,000 nl-sized droplets. Once the droplets were generated, the samples were transferred to a thermal cycler (C1000 Touch™ Thermal cycler) for PCR. Following the PCR, the plate containing the droplets was placed in a droplet reader (Bio-Rad, QX200 Droplet reader). he droplet reader's autosampler picks up droplets from each of the wells of the PCR plate, and fluorescence is measured for individual droplets. The abundance of the transcripts was obtained using the QuantaSoft™ Software. Transcript levels of *MPS1* were normalized against the corresponding transcript levels of *UBC6*.

Cell fixation for SIM microscopy

Cells containing the fluorescent markers for SBP analysis were elutriated as described earlier. For each time point, 1mL of cell culture was collected, pelleted, and washed in 1mL of PBS. Cells were then spun at 3,000rpm for 3 m in a microcentrifuge and resuspended in 1mL of 4% paraformaldehyde (Ted Pella, Inc.) in a 133mM sucrose in PBS solution. Fixation was for 15 min at room temperature, followed by two more washes in PBS. Cells were stored at 4°C until they were analyzed by microscopy.

SIM microscopy

Structured Illumination Microscopy analysis was performed on fixed cells, which had been mounted onto glass slides using ProLong Gold Antifade mountant (ThermoFisher Scientific). Mounted cells were stored in the dark at room temperature for 48 h prior to SIM analysis.

Images of Z-series (step size of 0.2 μm) of cells were collected using the Nikon Structured Illumination Super-Resolution Microscope fitted with a 100×1.46 NA objective. Images were captured in the 3D-SIM mode using NIS-Elements and SIM processing was performed using the SIM module in the Nikon software package. Image projections were made in Image-J software (National Institutes of Health).

ACKNOWLEDGEMENTS

This work was supported by NIH grants R01 GM123139 to M.P., P01 GM105537 to M.W. A.A. was supported by NIH T32 Oncogenic Signals and Chromosome Biology Training grant (T32 CA108459).

REFERENCES

Amberg, DC, Burke, DJ, and Strathern, JN (2006). Yeast protein extracts. CSH Protoc 2006, pdb. prot4152.

Aramayo, R, and Polymenis, M (2017). Ribosome profiling the cell cycle: lessons and challenges. Curr Genet 63, 959–964.

Aydogan, MG et al. (2020). An Autonomous Oscillation Times and Executes Centriole Biogenesis. Cell 181, 1566-1581.e27.

Aydogan, MG, Wainman, A, Saurya, S, Steinacker, TL, Caballe, A, Novak, ZA, Baumbach, J, Muschalik, N, and Raff, JW (2018). A homeostatic clock sets daughter centriole size in flies. J Cell Biol 217, 1233–1248.

Blank, HM et al. (2017). Translational control of lipogenic enzymes in the cell cycle of synchronous, growing yeast cells. EMBO J 36, 487–502.

Blank, HM, Callahan, M, Pistikopoulos, IPE, Polymenis, AO, and Polymenis, M (2018). Scaling of G1 Duration with Population Doubling Time by a Cyclin in Saccharomyces cerevisiae. Genetics 210, 895–906.

Blank, HM, Papoulas, O, Maitra, N, Garge, R, Kennedy, BK, Schilling, B, Marcotte, EM, and Polymenis, M (2020). Abundances of transcripts, proteins, and metabolites in the cell cycle of budding yeast reveal coordinate control of lipid metabolism. Mol Biol Cell 31, 1069–1084.

Boveri, T (2008). Concerning the origin of malignant tumours by Theodor Boveri. Translated and annotated by Henry Harris. J Cell Sci 121, 1–84.

de Bruin, RA, McDonald, WH, Kalashnikova, TI, Yates, J, 3rd, and Wittenberg, C (2004). Cln3 activates G1-specific transcription via phosphorylation of the SBF bound repressor Whi5. Cell 117, 887–898.

Bullitt, E, Rout, MP, Kilmartin, JV, and Akey, CW (1997). The yeast spindle pole body is assembled around a central crystal of Spc42p. Cell 89, 1077–1086.

Castillo, AR, Meehl, JB, Morgan, G, Schutz-Geschwender, A, and Winey, M (2002). The yeast protein kinase Mps1p is required for assembly of the integral spindle pole body component Spc42p. J Cell Biol 156, 453–465.

Cherry, JM et al. (2012). Saccharomyces Genome Database: the genomics resource of budding yeast. Nucleic Acids Res 40, D700-5.

Costanzo, M, Nishikawa, JL, Tang, X, Millman, JS, Schub, O, Breitkreuz, K, Dewar, D, Rupes, I, Andrews, B, and Tyers, M (2004). CDK activity antagonizes Whi5, an inhibitor of G1/S transcription in yeast. Cell 117, 899–913.

Creanor, J, and Mitchison, J (1979). Reduction of perturbations in leucine incorporation in synchronous cultures of Schizosaccharomyces pombe made by elutriation. J Gen Microbiol 112, 385–388.

Cross, FR (1988). DAF1, a mutant gene affecting size control, pheromone arrest, and cell cycle kinetics of Saccharomyces cerevisiae. Mol Cell Biol 8, 4675–4684.

Di Talia, S, Skotheim, JM, Bean, JM, Siggia, ED, and Cross, FR (2007). The effects of molecular noise and size control on variability in the budding yeast cell cycle. Nature 448, 947–951.

Friedman, DB et al. (2001). Yeast Mps1p phosphorylates the spindle pole component Spc110p in the N-terminal domain. J Biol Chem 276, 17958–17967.

Giaever, G et al. (2002). Functional profiling of the Saccharomyces cerevisiae genome. Nature 418, 387–391.

Gruber, AR, Lorenz, R, Bernhart, SH, Neuböck, R, and Hofacker, IL (2008). The Vienna RNA websuite. Nucleic Acids Res 36, W70-74.

Hardwick, KG, Weiss, E, Luca, FC, Winey, M, and Murray, AW (1996). Activation of the budding yeast spindle assembly checkpoint without mitotic spindle disruption. Science 273, 953–956.

Hartwell, LH, Culotti, J, Pringle, JR, and Reid, BJ (1974). Genetic control of the cell division

cycle in yeast. Science 183, 46–51.

Hartwell, LH, and Unger, MW (1977). Unequal division in Saccharomyces cerevisiae and its implications for the control of cell division. J Cell Biol 75, 422–435.

Ho, B, Baryshnikova, A, and Brown, GW (2018). Unification of Protein Abundance Datasets Yields a Quantitative Saccharomyces cerevisiae Proteome. Cell Syst 6, 192-205.e3.

Hoose, SA et al. (2012). A systematic analysis of cell cycle regulators in yeast reveals that most factors act independently of cell size to control initiation of division. PLoS Genet 8, e1002590.

Jaspersen, SL, and Winey, M (2004). The budding yeast spindle pole body: structure, duplication, and function. Annu Rev Cell Dev Biol 20, 1–28.

Johnston, GC, Pringle, JR, and Hartwell, LH (1977). Coordination of growth with cell division in the yeast Saccharomyces cerevisiae. Exp Cell Res 105, 79–98.

Jorgensen, P, Nishikawa, JL, Breitkreutz, BJ, and Tyers, M (2002). Systematic identification of pathways that couple cell growth and division in yeast. Science 297, 395–400.

Kaiser, C, Michaelis, S, Mitchell, A, and Cold Spring Harbor Laboratory. (1994). Methods in yeast genetics : a Cold Spring Harbor Laboratory course manual, Cold Spring Harbor, NY: Cold Spring Harbor Laboratory Press.

Lauzé, E, Stoelcker, B, Luca, FC, Weiss, E, Schutz, AR, and Winey, M (1995). Yeast spindle pole body duplication gene MPS1 encodes an essential dual specificity protein kinase. EMBO J 14, 1655–1663.

Li, S, Sandercock, AM, Conduit, P, Robinson, CV, Williams, RL, and Kilmartin, JV (2006). Structural role of Sfi1p-centrin filaments in budding yeast spindle pole body duplication. J Cell Biol 173, 867–877.

Litsios, A et al. (2019). Differential scaling between G1 protein production and cell size dynamics promotes commitment to the cell division cycle in budding yeast. Nat Cell Biol 21, 1382–1392.

Liu, X, and Winey, M (2012). The MPS1 family of protein kinases. Annu Rev Biochem 81, 561–585.

Longtine, MS, McKenzie, A, 3rd, Demarini, DJ, Shah, NG, Wach, A, Brachat, A, Philippsen, P, and Pringle, JR (1998). Additional modules for versatile and economical PCR-based gene deletion and modification in Saccharomyces cerevisiae. Yeast 14, 953–961.

Mair, P, and Wilcox, R (2016). Robust statistical methods in r using the wrs2 package. Harv Univ.

Michel, AM, Fox, G, M. Kiran, A, De Bo, C, O'Connor, PBF, Heaphy, SM, Mullan, JPA, Donohue, CA, Higgins, DG, and Baranov, PV (2014). GWIPS-viz: development of a ribo-seq genome browser. Nucleic Acids Res 42, D859–D864.

Nash, R, Tokiwa, G, Anand, S, Erickson, K, and Futcher, AB (1988). The WHI1+ gene of Saccharomyces cerevisiae tethers cell division to cell size and is a cyclin homolog. EMBO J 7, 4335–4346.

Nigg, EA, and Raff, JW (2009). Centrioles, centrosomes, and cilia in health and disease. Cell 139, 663–678.

Palframan, WJ, Meehl, JB, Jaspersen, SL, Winey, M, and Murray, AW (2006). Anaphase Inactivation of the Spindle Checkpoint. Science 313, 680–684.

Poch, O, Schwob, E, de Fraipont, F, Camasses, A, Bordonne, R, and Martin, RP (1994). RPK1, an essential yeast protein kinase involved in the regulation of the onset of mitosis, shows homology to mammalian dual-specificity kinases. Mol Gen Genet 243, 641–653.

Polymenis, M, and Aramayo, R (2015). Translate to divide: Control of the cell cycle by protein synthesis. Microb Cell 2, 94–104.

Polymenis, M, and Schmidt, EV (1997). Coupling of cell division to cell growth by translational control of the G1 cyclin CLN3 in yeast. Genes Dev 11, 2522–2531.

Pringle, JR, Hartwell, LH (1981). The Saccharomyces cerevisiae Cell Cycle. In: The Molecular and Cellular Biology of the Yeast Saccharomyces, Cold Spring Harbor Laboratory Press,

97–142.

Puig, O, Caspary, F, Rigaut, G, Rutz, B, Bouveret, E, Bragado-Nilsson, E, Wilm, M, and Seraphin, B (2001). The tandem affinity purification (TAP) method: a general procedure of protein complex purification. Methods 24, 218–229.

Soma, S, Yang, K, Morales, MI, and Polymenis, M (2014). Multiple metabolic requirements for size homeostasis and initiation of division in Saccharomyces cerevisiae. Microb Cell 1, 256–266.

Sudbery, PE, Goodey, AR, and Carter, BL (1980). Genes which control cell proliferation in the yeast Saccharomyces cerevisiae. Nature 288, 401–404.

Wilcox, RR (2011). Introduction to robust estimation and hypothesis testing, Academic press.

Winey, M, and Bloom, K (2012). Mitotic spindle form and function. Genetics 190, 1197–1224.

Winey, M, Goetsch, L, Baum, P, and Byers, B (1991). MPS1 and MPS2: novel yeast genes defining distinct steps of spindle pole body duplication. J Cell Biol 114, 745–754.

FIGURES

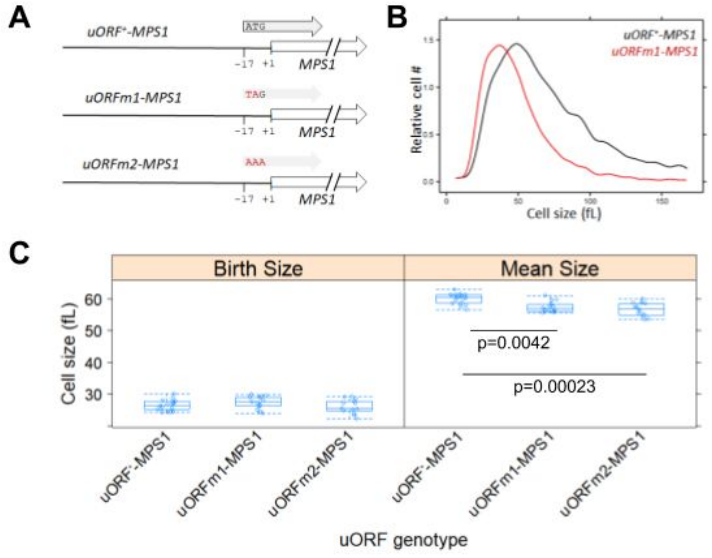

Figure 1. Mutating a conserved uORF in *MPS1* reduces cell size. A, Schematic of the *MPS1* locus in the strains used in this study to test the role of the *MPS1* uORF. **B**, Cell size histograms (size in fL, x-axis; number of cells, y-axis) for the indicated strains (*uORF*$^{+}$*-MPS1* [strain MSP240-3C] and *uORFm1-MPS1* [strain MSP241-1C]; see Materials and Methods) in otherwise wild type cells, cultured in rich medium (YPD), proliferating asynchronously and exponentially. **C**, Box-plots showing the mean and birth size of populations of cells from multiple independent measurements from the indicated strains (all in the W303 background, carrying TAP-tagged *MPS1* alleles; see Materials and Methods). The associated p-values were from the nonparametric Kruskal-Wallis and the posthoc Nemenyi tests (calculated with the PMCMR R language package) between the samples shown. The values used to generate the graphs in C are in supplementary File1/sheet 'fig1c'.

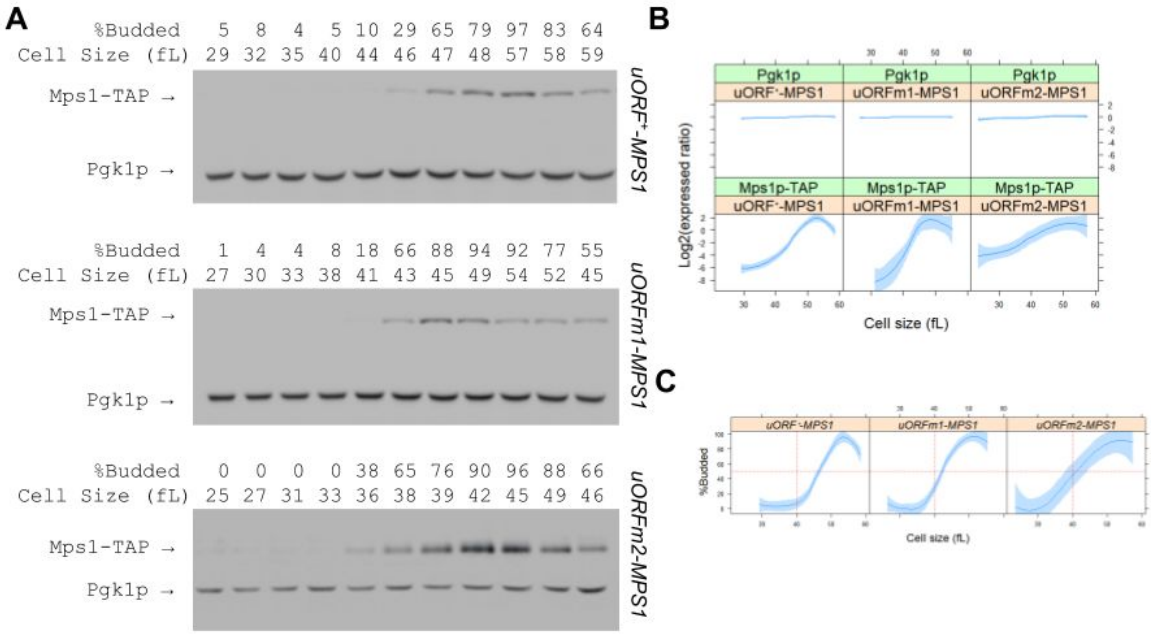

Figure 2. Mutating the *MPS1* uORF accelerates the appearance of Mps1p in the cell cycle and promotes Start. The abundance of Mps1p-TAP was monitored in wild type and *uORFm-MPS1* cells, constructed as described in Materials and Methods. Samples were collected by elutriation in a rich, undefined medium (YPD) and allowed to progress synchronously in the cell cycle. Experiment-matched loading controls (measuring Pgk1p abundance) were also quantified and shown in parallel. A, Representative immunoblots, along with the percentage of budded cells (%B) and the cell size (in fL), for each of the samples. B, From at least three independent experiments in each case, the Mps1p-TAP and Pgk1p signal intensities were quantified as described in Materials and Methods. The Log2(expressed ratios) values are on the y-axis, and cell size values are on the x-axis. Loess curves and the standard errors at a 0.95 level are shown. All the immunoblots for this figure are in supplementary File2, while the values used to generate the graphs are in supplementary File1/sheet 'fig2b' and sheet 'fig2c'.

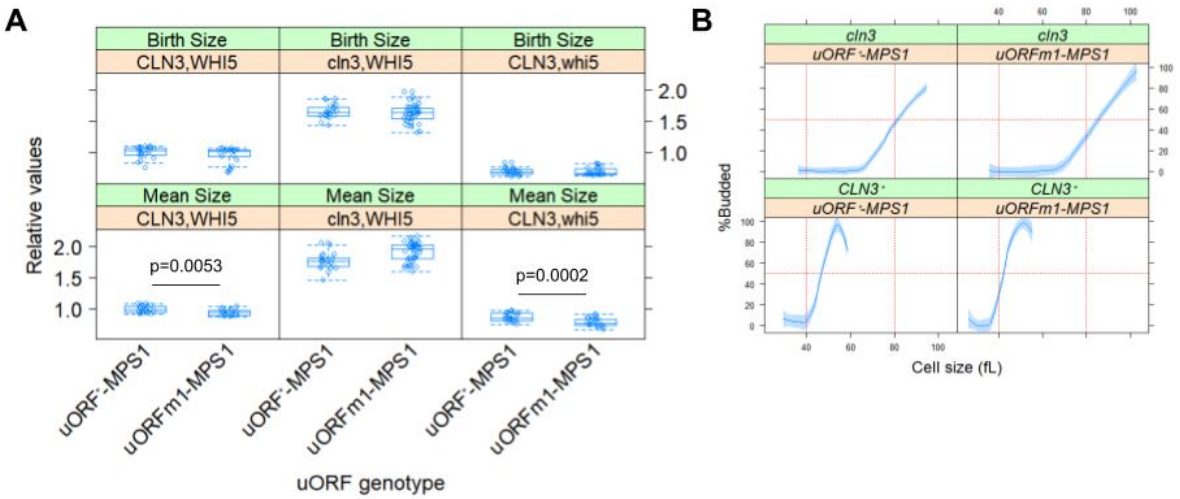

FIGURE 3. The smaller mean and critical size of *MPS1* uORF mutants depends on the G1 cyclin Cln3p. A, Box-plots showing the mean and birth size of populations of cells from multiple independent measurements from the indicated strains. The associated p-values from the non-parametric Wilcoxon rank-sum test between the two samples in each case are shown. **B**, Summary of cell cycle profiles of the indicated *MPS1* uORF genotype and strain background, done as in Figure 2. Loess curves and the standard errors at a 0.95 level are shown. The critical size is reduced by 9% (Wilcoxon rank sum test; p-value = 0.0005828) in *uORFm1-MPS1* cells, but there is no effect in *cln3Δ* cells. The values used to generate the graphs are in supplementary File1/sheet 'fig3a' and sheet 'fig3b'.

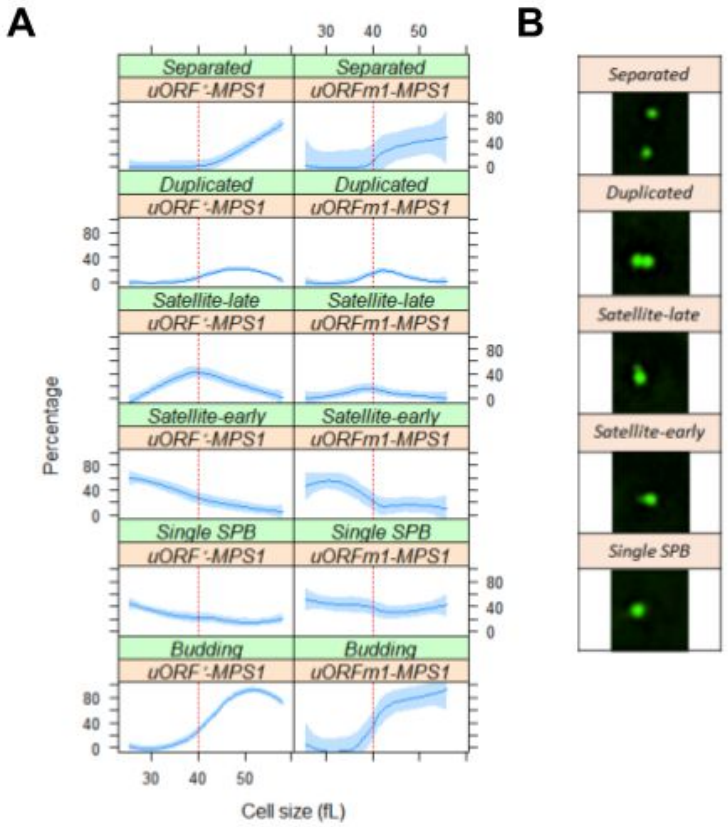

FIGURE 4. Reducing the translational efficiency of *MPS1* accelerates SPB duplication in synchronous, elutriated cells. A, Elutriated, early G1 daughter cells of the indicated *MPS1* uORF genotype carrying *SPC42-GFP* and *SPC110-tomato* alleles were monitored by SIM microscopy as they progressed synchronously in the cell cycle, in rich (YPD) medium. On the x-axis of each panel is cell size. On the y-axis is the percentage of cells with the indicated morphology, based on the fluorescence of SPB markers. Loess curves and the standard errors at a 0.95 level are shown. **B**, Representative SIM images of the SPB morphology, based on Spc42-GFP fluorescence, used to score the synchronous cells at various stages of the cell cycle. The values used to generate the graphs are in supplementary File1/sheet 'fig4a'.

```
                 uORF        M  I  S  K  Q  T  C  Q  Q  T  H  S  M  I  M  W  I  *
                Mps1p                          M  S  T  N  S  F  H  D  Y  V  D  L  K  S  R  T
SGD_Scer_MPS1/YDL028C      TGGATGATCTCAAAACAAACATGTCAACAAACTCATTCCATGATTATGTGGATTTAAAATCGAGAAC
                             -17             +1

                 uORF        M  T  S  K  Q  S  C  Q  Q  I  H  S  M  I  I  W  I  *
                Mps1p                          M  S  T  N  S  F  H  D  Y  M  D  L  K  S  R  T
     MIT_Spar_c96_3651     TGAATGACCTCAAAACAATCATGTCAACAAATTCATTCCATGATTATATGGATTTAAAGTCGAGAAC

                 uORF        M  S  S  I  *
                Mps1p                          M  S  T  N  S  F  H  D  Y  M  D  S  K  S  R  M
    MIT_Suva_c788_3655     TGAATGAGTTCAATATAATTATGTCAACAAATTCATTCCATGACTATATGGATTCAAAGTCGAGAAC

                 uORF        M  S  S  I  *
                Mps1p                          M  S  T  N  S  F  H  D  Y  M  D  S  K  S  R  M
WashU_Sbay_Contig554.19    TGAATGAGTTCAATATAATTATGTCAACAAATTCATTCCATGACTATATGGATTCAAAGTCGAGAAC

                 uORF        M  S  S  K  K  L  C  R  Q  I  H  S  M  T  I  W  I  Q  N  R  K  *
                Mps1p                          M  S  T  N  S  F  H  D  Y  M  D  S  K  S  K  M
WashU_Skud_Contig1646.3    TGAATGAGCTCCAAAAAATTATGTCGACAAATTCATTCCATGACTATATGGATTCAAAATCGAAAAT
```

Figure S1. The initiation position of a uORF in the *MPS1* transcript, but not the length or the sequence of the uORF-encoded peptide, is conserved in the *Saccharomyces* genus. The genomic DNA sequence for *S. cerevisiae* (top) and for the related species are shown (as listed on the Saccharomyces Genome Database (SGD) fungal sequence alignments (Cherry *et al.*, 2012)). Above each DNA sequence, the sequences of the uORF-encoded peptides and the amino-terminal sequence of Mps1p are shown.

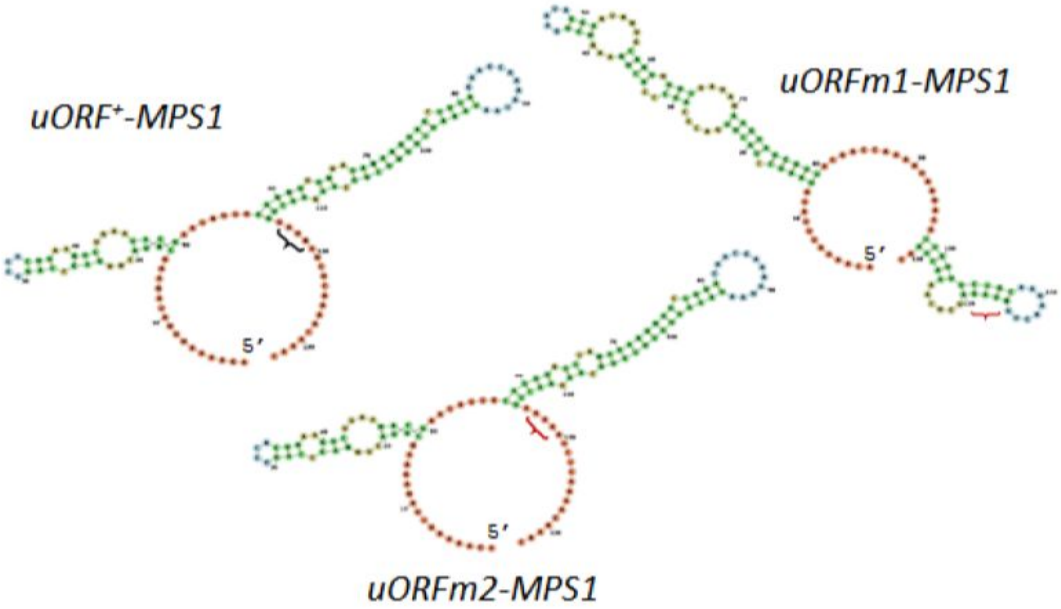

Figure S2. Predicted RNA structure of the *MPS1* 5'-leader in each of the strains shown. The predicted structures were the minimum free energy (MFE) ones calculated with the Vienna RNA Websuite (Gruber *et al.*, 2008). The brackets indicate the position of the start codon of the uORF in each case.

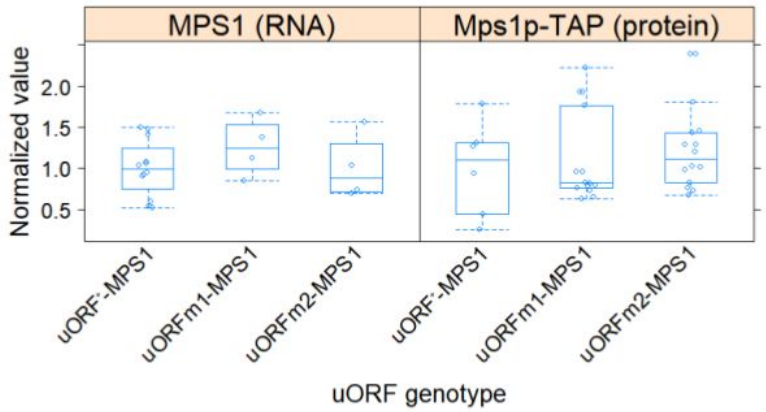

Figure S3. Mutating the *MPS1* uORF does not change significantly the steady-state abundance of Mps1p in asynchronous cells. The box-plots show the levels of *MPS1* mRNA (left panel) and Mps1p protein (right panel) from multiple independent experiments, measured as described in Materials and Methods. The values were normalized against both Pgk1p levels in each sample and total protein, using the Mini-PROTEAN® TGX Stain-Free™ Gels, as described in Materials and Methods. All the immunoblots for this figure are in supplementary File3, while the values used to generate the graphs are in supplementary File1/sheet 'figs3'.